Journal of Applied Electrochemistry **30**: 777–786, 2000.

Design equations for optimized PEM fuel cell electrodes

C.C. BOYER[1,*], R.G. ANTHONY[1] and A.J. APPLEBY[2]
[1]*Department of Chemical Engineering, Texas A&M University, College Station, TX 77843-3122, USA*
[2]*Center for Electrochemical Systems and Hydrogen Research, Texas A&M University, College Station, TX 77843-3402, USA*
*(*author for correspondence: Lynntech, Inc., 7610 Eastmark Dr., College Station, TX 77845, USA)*

Received 19 July 1999; accepted in revised form 8 February 2000

Key words: effectiveness, electrode, fuel cell, optimization

Abstract

This paper presents simple mathematical expressions that can be used for optimizing fuel cell electrode structures, specifically polymer electrolyte membrane fuel cells (PEMFCs). Based on the effectiveness factor, equations relate current density to catalyst utilization and a mass transfer coefficient. These can be used to screen new materials or identify which specific processes need to be improved in an existing electrode design. The optimum thickness, or catalyst loading, and maximum current that can be achieved with a given set of materials can be calculated from a simple set of equations based on the mass transfer characteristics of the electrode materials. These methods can save considerable experimental time and cost during electrode development.

List of symbols

a	surface area per volume ($cm^2\ cm^{-3}$)
b	effective Tafel slope (mV)
c	molar concentration ($mol\ cm^{-3}$)
D	effective diffusivity ($cm^2\ s^{-1}$)
F	Faraday's constant ($C\ equiv^{-1}$)
H	Henry's constant ($atm\ cm^3\ mol^{-1}$)
i	electrode current flux or current density ($A\ cm^{-2}$)
k	electrokinetic rate constant ($A\ cm^{-2}\ atm^{-1}$)
L	thickness of catalyst layer (cm)
n	charge equivalents per mol
P	pressure (atm)
R	resistance ($\Omega\ cm^2$)
V	electric potential (V)
x	molar fraction
Z	effectiveness factor

Greek symbols

α	inherent mass transfer rate ($A\ cm^{-2}$)
β	mixed inherent mass transfer rate
δ	effective agglomerate depth (cm)
ε	volume fraction
ϕ	rate modulus, kinetic rate/mass transfer rate
η	overpotential (V)
κ	effective conductivity ($S\ cm^{-1}$)
ν	intrinsic kinetic rate ($A\ cm^{-2}$)
ρ	density ($g\ cm^{-3}$)
σ	migration inherent mass transfer rate ($A\ cm^{-2}$)
ω	dummy variable

Subscripts

aggl	agglomerate
cat	catalyst active layer
film	film covering agglomerates
mem	membrane layer
migr	migration
pore	gas pores
diff	diffusion

1. Introduction

To move proton exchange membrane fuel cells (PEMFCs) from the proof-of-concept stage into commercialization, research efforts will require a rapid and convenient means to optimize electrode structures, especially as new materials become available [1]. Experimental optimization studies are time intensive and include high uncertainty [2, 3]. A number of PEMFC operating models have been published in the literature [4–10]. In general, these are not sufficiently transparent to allow simple expressions to be used for optimization of components, and in some cases, they make assumptions that are physically limiting, or even phenomenologically unlikely. The objective of this paper is to use the same physical principles as previously published models, and to derive from them some useful approximate expressions to allow optimization in the laboratory. First, a method is shown which can evaluate existing electrodes and new materials by determining the relative effective-

ness of each individual mass transfer process. Then, equations are developed which calculate the maximum current obtainable and the optimum electrode active layer thickness for a given set of electrode materials and operating conditions. Finally, the validity of the equations is demonstrated by applying them to polymer electrolyte electrodes with contemporary materials.

From a commercial perspective, a fuel cell should be designed with the highest power per unit cost, power per unit volume, fuel efficiency, reliability and lifetime. Maximum power per unit volume is usually achieved by obtaining the maximum power in each cell. Maximum power per unit cost is achieved by obtaining the maximum power and maximum catalyst utilization in each cell. Efficiency usually targets an average operating voltage for the cell. Cell reliability and lifetime requirements place constraints on the electrode design. Each fuel cell application requires weighting the importance of these characteristics differently. Before electrode optimization can begin, the operational goals and constraints must be defined.

This work is based on models for different types of fuel cells that have been published in the literature [4–23]. In general, they use macroscopic processes to describe transport through the depth of the electrode, and microscopic processes that describe transport and reactions at a local point, as shown in Figure 1. The essential processes are represented by the following parameters: reactant diffusivity through the substrate; reactant diffusivity through the active layer; proton conductivity through the active layer; proton conductivity through the electrolyte separator; electronic conductivity through the current collector; electronic conductivity through the active layer; volumetric kinetic rate in the active layer; and a microscopic parameter to describe the local reactant diffusivity into regions filled with electrolyte in the active layer.

The ability to mathematically characterize complex transport and kinetic processes in multiphase materials limits the accuracy of models. Due to the complex geometry of porous media, the transport equations are volume averaged with an apparent parameter that emulates the process for a simplified, linear geometry. This paper takes the most simple approach in which each transport process in the electrode has only one parameter associated with it; the constitutive equation for diffusion flux is described by Fick's law, and the equation for migration flux is described by Ohm's law. It assumes isotropic kinetic and transport properties in each layer. In this paper the agglomerate model will describe the microscopic diffusion process. This approach is a simplification, but it appears to be adequate for PEMFCs, which are the primary focus of this paper. Electrical resistance losses were neglected here because the carbon used to support the catalyst at the present time has sufficient electrical conductivity ($\sim$1.0 S cm^{-1} [21]). The model assumes steady-state operation without problems such as drying, flooding, reactant crossover, electrical shorting, or catalyst poisoning. With these assumptions in mind, one realizes that this analysis is a first-cut approximation; more accurate optimization calculations will require a more rigorous model and detailed experimental characterization. However, a more complicated model [16] will entail many more parameters which may be very difficult to characterize, so that the results may not justify the effort.

The following evaluations depend on prior knowledge of the kinetic and mass transfer parameters associated with the electrode materials and construction. These can be obtained from a number of experimental techniques described in the literature such as fitting polarization curves [17–21], fitting a.c. impedance data [22–24], layered experiments [25, 26], microelectrode experiments [27, 28], current pulse data [29], and potential decay curves [30]. As materials and operating conditions change, experimental characterization of the materials followed with the methods described in this paper provide a quick and efficient means to obtain optimized electrodes.

2. Development of optimization equations

2.1. *Identifying relative transport losses and screening new materials*

For maximum power and catalyst utilization at lowest cost, an electrode should be designed such that all the

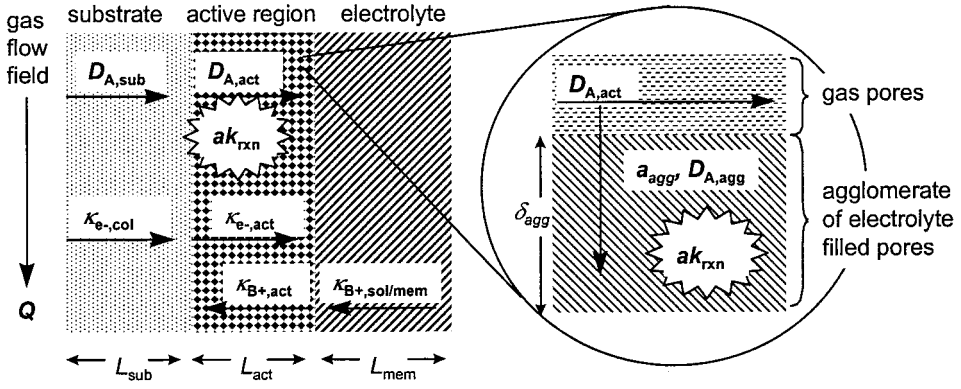

Fig. 1. Physical picture of the fuel cell electrode model at the macrolevel and the microlevel as described by a thin film covered agglomerate.

transport and kinetic processes in the cell are balanced, that is, no single process is more rate-limiting than the others. As used previously in the literature [31, 32], one way to quantify the extent that a mass transfer process limits a given system is via the use of an 'effectiveness factor', Z. The effectiveness of a material based on its transport properties can be compared to the effectiveness of other materials to see if it is a viable candidate for electrode construction.

This effectiveness factor is the ratio of the actual current obtained with mass transfer limitations to the intrinsic kinetic current that would be obtained if there were no mass transfer limitations. It can also be thought of as a measure of catalyst utilization. It is a function of the dimensionless rate modulus, ϕ, which is defined as the intrinsic kinetic rate, v, divided by the inherent mass transfer rate, α, both in A cm^{-2} units. The square root of the rate modulus as defined here is commonly known in heterogeneous catalysis as the Theile modulus. It is defined here without the square root, because the functionality of the non-active layer processes do not require it. Hence,

$$Z \equiv \frac{i}{v} = f[\phi] \tag{1}$$

where the rate modulus is $\phi = (v/\alpha) \equiv$ (intrinsic kinetic rate/inherent mass transfer rate), and i is the actual current density. The effectiveness factors for individual transport processes are summarized in Table 1 and are plotted in Figure 2.

The activity of the catalyst, reactant concentration, and potential in the active region determine the intrinsic kinetic current. This manuscript will only consider first order kinetic reactions, as in the PEMFC hydrogen and oxygen electrodes. The Tafel equation sufficiently describes the kinetic rate as a function of potential within the operating range of most fuel cell electrodes. The Tafel slope may (and for oxygen indeed does [33]) change as a function of potential due to the complex reaction mechanism and the adsorption characteristics of the intermediates. However, the use of the Tafel equation is still valid for the equations presented here because they deal with only small perturbations around a given potential within the thickness of a thin porous electrode.

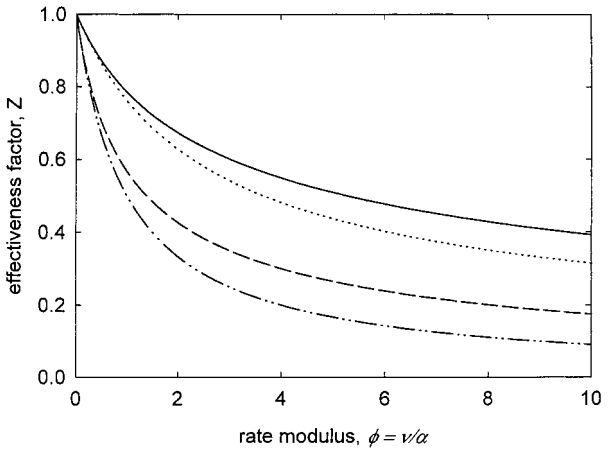

Fig. 2. Mass transfer limitation as a function of the rate modulus for transport processes in the MEA: proton transport in the active region, oxygen transport in the active region, proton transport in the membrane and oxygen transport in the substrate. Key: (——) migration in catalyst layers; (- - - -) diffusion in catalyst layer; (— —) migration in membrane; (— ··) diffusion in substrate.

The intrinsic kinetic current flux of the electrode is a function of the potential, V, with respect to a reference electrode, the apparent local Tafel slope, b, the reactant gas partial pressure, $x_A P$, (or molar concentration in liquid systems), the activity of the catalyst surface, k, the active platinum surface area per unit volume, a_{cat}, and the depth of the active region, L. Hence,

$$v = x_0 P a_{\text{cat}} L K \exp[V/b] \tag{2}$$

The inherent mass transfer rate is determined from the dimensionless material balances for a particular process, and depends on the type of mass transport mechanism involved. The effectiveness factor of a mass transport process comes from the analytical solution of the volume averaged material balance, which considers only the kinetic rate and a particular mass transport process.

To make improvements to an electrode, it is important to identify rate-limiting processes and know what level of transport is required to obtain a performance

Table 1. Summary of effectiveness factors for transport processes

Transport mechanism	Inherent mass transfer rate	Effectiveness factor, Z
Gas diffusion in active region	$\alpha_{\text{cat,pore}} = \dfrac{nFx_0 cD_{\text{A}}^{\text{cat}}}{L_{\text{cat}}}$	$Z_{\text{cat,pore}} = \dfrac{\tanh[\sqrt{\phi}]}{\sqrt{\phi}}$
Gas diffusion in agglomerates	$\alpha_{\text{cat,agg}} = \dfrac{a_{\text{agg}} L_{\text{cat}} nFx_0 PD_{\text{A}}^{\text{agg}}}{H_{\text{A}} \delta_{\text{agg}}}$	$Z_{\text{cat,agg}} = \dfrac{\tanh[\sqrt{\phi}]}{\sqrt{\phi}}$
Gas diffusion in catalyst film	$\alpha_{\text{cat,film}} = \dfrac{a_{\text{film}} L_{\text{cat}} nFx_0 PD_{\text{A}}^{\text{film}}}{H_{\text{A}} \delta_{\text{film}}}$	$Z_{\text{cat,film}} = \dfrac{1}{1+\phi}$
Proton migration in active region	$\alpha_{\text{cat,migr}} = \dfrac{\kappa_{\text{H}^+}^{\text{cat}} b}{L_{\text{cat}}}$	$Z_{\text{cat,migr}} = \dfrac{\sin[\bar{\omega}]}{\sqrt{\phi/2}}, \varpi = \sqrt{\dfrac{\phi}{2}}\cos[\varpi]$
Gas diffusion through substrate	$\alpha_{\text{sub}} = \dfrac{nFx_0 cD_{\text{A}}^{\text{sub}}}{L_{\text{sub}}}$	$Z_{\text{sub}} = \dfrac{1}{1+\phi}$
Proton migration in membrane	$\alpha_{\text{mem}} = \dfrac{\kappa_{\text{H}^+}^{\text{mem}} b}{L_{\text{mem}}} = \dfrac{b}{R_{\text{mem}}}$	$Z_{\text{mem}} = \exp[-Z_{\text{mem}}\phi]$

goal. For this purpose, the effectiveness factor equations have been rearranged to relate the current density and inherent mass transfer rate to the individual effectiveness of a mass transfer process without the need to know the intrinsic kinetic rate. The current generated as a function of catalyst utilization for a single limiting mass transfer process can be determined from the inherent mass transfer rate and the effectiveness factor by expressing the intrinsic kinetic rate as $v = \alpha\phi$ and substituting it into the equation $i = vZ$. The inverse of the effectiveness factor function will give the rate modulus, ϕ, as a function of the effectiveness, Z, that is,

$$i = \alpha Z\ \phi(Z) = f(\alpha, Z) \tag{3}$$

The effectiveness of a mass transfer process can be determined as a function of the operating current density by rearranging Equation 3 to give the product of the effectiveness factor and rate modulus as a function of the current density and inherent mass transfer rate, that is

$$\alpha = \frac{i}{Z\ \phi(Z)} = f(i, Z) \tag{4}$$

The effectiveness factor can be determined from the product of the effectiveness factor and rate modulus by graphical or iterative methods. Thus,

$$Z = f(Z\,\phi) = f(i, \alpha) \tag{5}$$

This analysis can be applied to the cathode with oxygen from air, and to the anode with hydrogen from reformate or methanol in water. Table 2 shows an example of how the relative rates compare for each type of process. In the first column, values are given for the current density from Equation 3 corresponding to an effectiveness of one-half when the inherent mass transfer rate is equal to 1 A cm^{-2}. This quantitative analysis is useful for determining the current that might be achieved by a given material and electrode design. The second column contains the effectiveness of each process from Equation 5 at a current density of 0.5 A cm^{-2} with an inherent mass transfer rate equal to 1 A cm^{-2}. This comparative analysis may be used to determine which processes are rate limiting. The third column contains the inherent mass transfer rate required from Equation 4 to achieve a current of 1.0 A cm^{-2} at an effectiveness of 0.5. This may be used to determine the necessary transport rates for a given performance goal. While each of the individual effectiveness factors have a true physical meaning, there is unfortunately no simple correlation between the overall electrode effectiveness and the individual effectiveness factors, since all the processes are interactive and simultaneous.

The active region has several transport processes that should be balanced in an optimized electrode: ionic conductivity, electronic conductivity and reactant diffusion. Because fuel cell electrodes are multiphase structures, increasing the transport facility of one process by increasing its phase volume usually decreases the transport facility of the other processes. Optimization involves searching for the correct ratio of materials in the composite layer (unless there is an optimizing constraint such as material cost or conflict of fabrication capabilities).

2.2. *Optimum active layer thickness*

The thickness, or catalyst loading, in the active layer is an important consideration of electrode design. Generally, fuel cells are designed to operate at a given potential to meet an efficiency goal. At constant potential, the current density will increase with catalyst loading until some point where mass transfer becomes rate limiting.

Exact analytical expressions show the maximum current and optimum thickness of an active layer when only one mass transfer process is significant. For the gas diffusion in the active layer pores, the term $Z = \tanh[\sqrt{\phi}]/\sqrt{\phi}$ approaches $1/\sqrt{\phi}$ when ϕ is greater than four. At this point, the equation for the current has a simple expression that is independent of layer thickness:

$$i_{\text{max, diffusion}} = \sqrt{\alpha v} = x_0\sqrt{nFcDPa_{\text{cat}}k\ \exp[\eta/b]} \tag{6}$$

In this region of operation there is an apparent doubling of the Tafel slope due to mass transfer [14]. The maximum current is proportional to the reactant gas fraction and proportional to the pressure or square root of the pressure depending on the diffusion mechanism. Molecular gas diffusion will exhibit square root pressure dependence. Knudsen diffusion or liquid diffusion will exhibit a first order pressure dependence.

Figure 3(a) shows the current and catalyst effectiveness as a function of active layer thickness. The layer thickness corresponding to a rate modulus of 4.0 achieves 97% of the maximum current density that would be obtained from an infinitely thick active layer.

Table 2. Evaluation of currents, effectiveness factors, and inherent transfer rates for the transport processes with hypothetical values

Transport process	Current/A cm^{-2} at Z = 1/2 α = 1 A cm^{-2}	Effectiveness at i = 0.5 A cm^{-2} α = 1 A cm^{-2}	Transfer rate/A cm^{-2} at i = 1 A cm^{-2} Z = 1/2
Migration in catalyst	2.5	0.85	0.40
Diffusion in catalyst	1.84	0.84	0.54
Migration in membrane	0.693	0.61	1.4
Diffusion in substrate	0.5	0.5	2.0

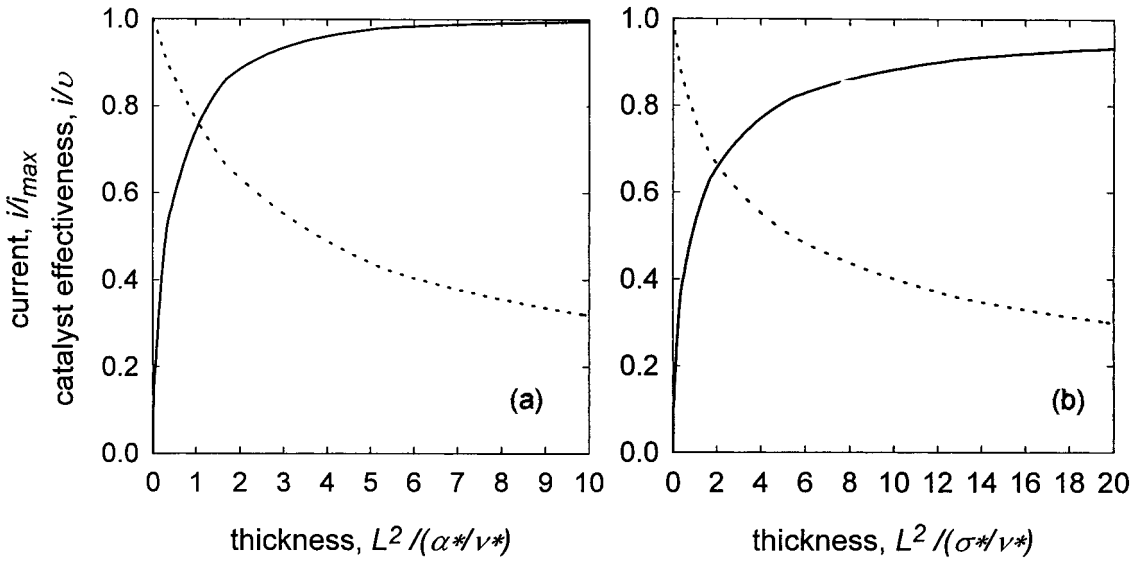

Fig. 3. Current density increases and catalyst utilization decreases as the active layer thickness increases for (a) gas pore diffusion and (b) ion migration. Key: (——) current; (- - - -) effectiveness.

Catalyst utilization at this point is just less than one-half. The criterion for optimum thickness here was a compromise between maximum current density and maximum catalyst utilization. Hence,

$$L_{\text{opt, diffusion}} = 2\sqrt{\frac{\alpha^*}{\nu^*}} = 2\sqrt{\frac{nFcD}{Pa_{\text{V}}k\,\exp[\eta/b]}} \tag{7}$$

The starred variables represent the variable without the layer thickness, L. One might choose a different optimum thickness to achieve a slightly higher current density at much lower catalyst utilization, or higher catalyst utilization at a lower current density. The optimum thickness is independent of the reactant mole fraction and independent of pressure for Knudsen and liquid diffusion, but is inversely proportional to the square root of the pressure for molecular diffusion.

The affect of agglomerate diffusion can easily be added to the pore diffusion model by recognizing that the agglomerate effectiveness is independent of oxygen concentration and layer thickness. The product of the intrinsic kinetic rate and the agglomerate effectiveness factor replaces the intrinsic kinetic rate:

$$\begin{aligned} i_{\text{max, diff+aggl}} &= \sqrt{\alpha\nu Z_{\text{aggl}}} \quad \text{and} \\ L_{\text{opt, diff+aggl}} &= 2\sqrt{\frac{\alpha^*}{\nu^* Z_{\text{aggl}}}} \end{aligned} \tag{8}$$

If the agglomerate rate modulus is such that $\phi_{\text{agg}} > 4$, then $Z_{\text{agg}} = 1/\sqrt{\phi_{\text{agg}}}$ and

$$\begin{aligned} i_{\text{max, diff+aggl}} &= \sqrt{\alpha\nu^{1/2}\alpha_{\text{aggl}}^{1/2}} \quad \text{and} \\ L_{\text{opt, diff+aggl}} &= 2\sqrt{\frac{\alpha^*}{\nu^{*1/2}\alpha_{\text{aggl}}^{*1/2}}} \end{aligned} \tag{9}$$

When proton or electron resistance is the only significant mass transfer loss, the term $Z = \sin[\omega]/\sqrt{\phi/2}$ approaches $1/\sqrt{\phi/2}$ when $\phi/2$ becomes greater than 9.0. At this point, the current reaches a maximum independent of the active layer thickness:

$$i_{\text{max, migration}} = \sqrt{2\sigma\nu} = \sqrt{2\kappa b x_0 Pa_{\text{V}} k\,\exp[\eta/b]} \tag{10}$$

where the inherent mass transfer rate for migration will be represented by σ throughout the rest of this paper. The layer thickness at $\phi/2$ equal to 9.0 corresponds to a catalyst utilization of slightly less than 1/3 and to 93% of the current obtainable from an infinitely thick electrode, as is shown in Figure 3b. Then,

$$L_{\text{opt, migration}} = 3\sqrt{\frac{2\sigma^*}{\nu^*}} = 3\sqrt{\frac{2\kappa b}{x_0 Pa_{\text{cat}} k\,\exp[\eta/b]}} \tag{11}$$

Since the agglomerate effectiveness factor changes as the potential changes through the electrode layer, a simple solution for the agglomerate affect does not exist. The average intrinsic kinetic rate is lowered by a fraction of the initial agglomerate effectiveness factor (at $z = 1$) and this can be approximated by multiplying a reduced power of the agglomerate effectiveness to the intrinsic kinetic rate, that is,

$$\begin{aligned} i_{\text{max, migr+aggl}} &= \sqrt{2\sigma\nu Z_{\text{aggl}}^{3/4}} \quad \text{and} \\ L_{\text{opt, migr+aggl}} &= 3\sqrt{\frac{2\sigma^*}{\nu^* Z_{\text{aggl}}^{3/4}}} \end{aligned} \tag{12}$$

The above cases investigate optimum thickness when only one macroscopic mass transfer process is limiting; however, realistically, migration and diffusion are both significant mass transfer losses. When the sources of moving species (H^+ and O_2) come from opposite sides of

an active layer, as in the fuel cell, increasing the layer thickness beyond an optimum will cause a loss in performance. Figure 4 contains a numerical solution to the current density generated by a fuel cell cathode as a function of active layer thickness at different electrode potentials. In this calculation, the inherent mass transfer coefficients for migration and pore diffusion were equal and microscopic diffusion was neglected. A peak current density appears at the optimal thickness, which changes as a function of potential (or intrinsic kinetic rate), showing that electrodes must be optimized at a specific potential.

An exact analytical solution for the maximum current density and optimum layer thickness was not found with both processes. However, a geometric average of the individual solutions yields empirical rules that fit the maximum current density and optimum layer thickness obtained from the rigorous numerical solution. A plot of i_{max} against L_{opt} from these equations is also plotted on Figure 4 and labeled as the 'optimum design line'. It can be seen from these equations that as one or the other mass transfer coefficient becomes dominant, the limiting cases discussed earlier are obtained. The maximum current density generated from the active layer with ion migration, reactant diffusion in the pores, and reactant diffusion into agglomerates is given by:

$$i_{max} = \sqrt{\beta_1 v Z_{aggl}} \tag{13}$$

where

$$\beta_1 = \frac{2\sigma\alpha}{\left(\sqrt[2/3]{2\sigma} + \sqrt[2/3]{\alpha Z_{aggl}^{1/4}}\right)^{3/2}}$$

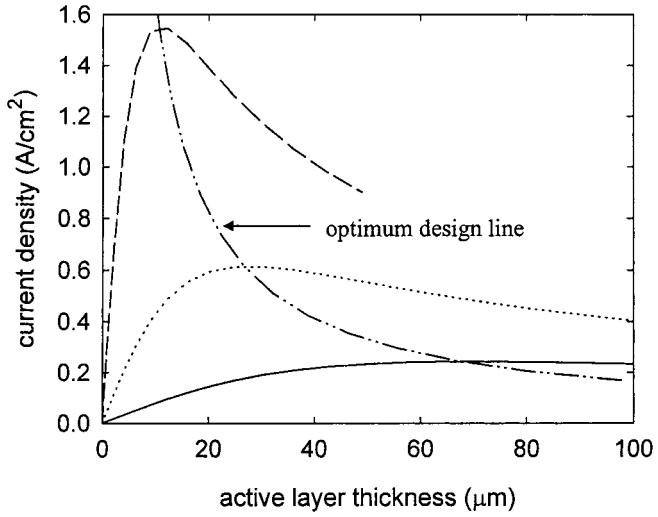

Fig. 4. A maximum current density appears as a function of active layer thickness when both migration and diffusion are limiting. Graph calculated by a numerical model for electrode potentials of $E = 0.8$, 0.75, and 0.7 V vs SHE with parameters $v^* = 1.0 \times 10^{-5} \exp((1.23 - E)/0.027)$ A cm^{-3}, $\sigma^* = 1.5 \times 10^{-3}$ and $\alpha^* = 1.5 \times 10^{-3}$ A cm^{-1}. The 'optimum design line', i_{max} against L_{opt}, was calculated from Equations 13 and 14. Key: (——) 0.8 V; (· · ·) 0.75 V; (– – –) 0.7 V; (–·–·–) i_{max} against L_{opt}.

The layer thickness where the maximum current density occurs is at

$$L_{opt} = 3\sqrt{\frac{\beta_2}{v^* Z_{aggl}}} \tag{14}$$

where

$$\beta_2 = \frac{2\sigma^*\alpha^*}{\left(\sqrt[2/3]{\frac{9}{2}\sigma^*} + \sqrt[2/3]{\frac{\alpha^*}{Z_{aggl}^{1/4}}}\right)^{3/2}}$$

The electrode substrate and electrolyte membrane contribute mass transfer losses. The membrane resistance lowers the available overpotential in the active layer, which drops the reaction activity, v. Increasing resistance increases the optimum thickness and decreases the maximum current exponentially. The parameters α, α_{agg} and v are proportional to the reactant concentration, which is altered by diffusion losses in the substrate. When diffusion dominates the losses in the active layer, losses from the substrate do not affect the optimum thickness of the active layer, and the maximum current density falls with the square of reactant concentration reaching the active layer. When migration limitations dominate, substrate losses increase the optimum thickness of the active layer, and decrease the maximum current linearly with concentration; that is,

$$\alpha = \left(1 - \frac{i}{\alpha_{sub}}\right)\alpha_0$$

$$\alpha_{aggl} = \left(1 - \frac{i}{\alpha_{sub}}\right)\alpha_{aggl,0} \tag{15}$$

$$v = \left(1 - \frac{i}{\alpha_{sub}}\right)\exp\left[-\frac{i}{\sigma_{mem}}\right]v_0$$

Because knowledge of the current density is required to obtain the corrected active layer parameters, an iterative approach must be used.

3. Results and discussion

3.1. *Optimum layer thickness*

The maximum current and optimum thickness equations described above were compared with results obtained from testing polymer electrolyte membrane fuel cell cathodes. Eight membrane and electrode assemblies (MEAs) were manufactured with all elements the same except for the platinum loading in the cathode. The loadings used were 0.076, 0.142, 0.231, 0.318, 0.421, 0.528, 0.638, and 0.736 mg Pt cm^{-2}. The catalyst layer which contained 20 wt % platinum on carbon support (Johnson Matthey) and 33 wt % Nafion^{TM} (DuPont de

Nemours) was painted onto a carbon cloth impregnated with acetylene black and Teflon^{TM}, then hot pressed to a Nafion^{TM} 112 membrane with the anode on the other side. The 5 cm^2 cells were tested at 50 °C and atmospheric pressure with humidified gases at a high enough flow rate to keep the oxygen concentration constant across the entire electrode area.

The cell current density versus platinum loading in the active layer is plotted along lines of constant cell potential in Figure 5. A clear trend shows how the current increases with increased platinum loading until a point where mass transfer becomes limiting. A deviation in the trend is seen at the cell with the thickest active layer, because its MEA was over-compressed during the hot press step of fabrication. This cell shows a lower ionic resistance because the membrane was thinned (higher currents with oxygen), some electrical shorting through the membrane (a shunt, giving lower current at high potential), and a higher oxygen mass transfer resistance because the pore structure was crushed (lower currents with air).

Transport and kinetic parameters for a cell of this construction have been estimated from the literature or measured using techniques described in the literature, and are listed in Table 3. Using these parameters with Equations 13 and 14 and correcting for the substrate and membrane resistance using Equation 15, the design line for the maximum current and optimum thickness can be evaluated for both oxygen and air cases. The calculations are compared with the experimental results in Figure 5. The layer thickness, L as used in the equations, is related to the catalyst loading, L as used in the experiments, by the density of the catalyst. The design calculations legitimately emulate the experimental results.

Table 3. Parameters used for calculating the maximum current and optimum cathode thickness plotted in Figure 5

Parameter	Value	Reference/method
E_0	1.23 V	21
b	0.03 V	21, 27
akP_0	6×10^{-6} A cm^{-3}	21, 27
$4FcD_{oxy}^{cat,pore}$	0.08 A cm^{-1}	method as in 19
$b\kappa_{H^+}^{cat}$	0.006 A cm^{-1}	18
$a_{agg}4FP_0D_A^{agg}/(H_A\delta_{agg})$	500 A cm^{-3}	experimental fit in 35
b/R_{mem}	0.222 A cm^{-2}	HF a.c. impedance
$4FcD_{oxy}^{sub}/L_{sub}$	15 A cm^{-2}	method as in 13
ρ_{cat}	150 mg Pt cm^{-3}	measured mass/volume

3.2. *Optimum Nafion content*

Table 4 shows the individual effectiveness factors of each process calculated with Equation 5 for the type of cathodes tested experimentally while operating on air at a current of 0.6 A cm^{-2} and containing an active layer thickness of 42 μm (0.63 mg Pt cm^{-2} was the optimum loading at that current). This analysis showed that the membrane was the largest loss in the fuel cell (i.e., it had the lowest effectiveness). The second largest loss was the proton resistance in the active layer with an effectiveness of 0.38. Diffusion into the agglomerates was the largest diffusion loss in the cell. Efforts to make better electrodes should focus on improving these mass transfer processes.

Increasing the polymer content in the active layer could improve the proton conductivity. In another study [34], the transport and kinetic parameters in the cathode active layer containing platinum dispersed on Vulcan black XC-72 (E-Tek) were characterized as a function of the ionomer content. Those results are summarized in Table 5 for a cathode operating with air at 50 °C. Typically, the substrate has a diffusion parameter around $\alpha_{sub} = x_{oxy}$ 12 A cm^{-2} and the Nafion 112 membrane had a migration parameter $\sigma_{mem} =$ 0.13 A cm^{-2}.

Figure 6 shows how the maximum obtainable current and the optimum catalyst loading change as a function

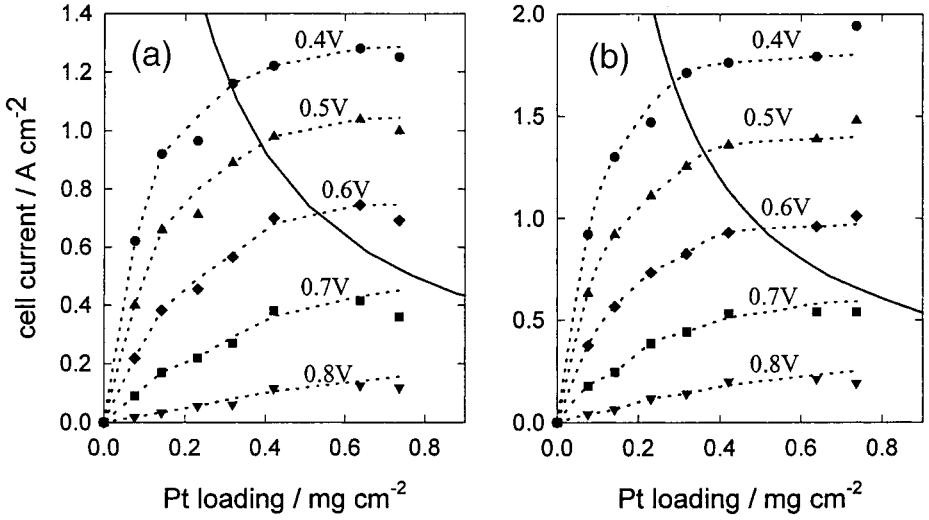

Fig. 5. Experimental current density shown as a function of platinum loading along lines of equal cell potential to compare with the design equations for (a) hydrogen/air and (b) hydrogen/oxygen. The 5 cm^2 cells were tested at $T = 50$ °C, $P = 1$ atm, with humidified gases at high stoichiometry. The solid line is the calculated i_{max} against L_{opt} as described in the text.

Table 4. Effectiveness for each process in the cathode of the experimentally tested cells at a current of 0.6 A cm^{-1} and an active layer thickness of 42 μm

Mass transfer process	Effectiveness factor
Migration in membrane	0.09
Migration in active layer	0.38
Diffusion in agglomerate	0.62
Diffusion in substrate	0.81
Diffusion in pores of active layer	0.97

of wt % Nafion^{TM} in the active layer for air operation with a 20% Pt/C catalyst. The equations predict an optimum maximum current density of 0.38 A cm^{-2} at 0.7 V (56% fuel efficiency) with a cathode loading of 0.39 mg Pt cm^{-2}, 60 wt % Nafion^{TM}, a membrane resistance of 0.2 Ω cm^2, and a substrate limiting current of 2.4 A cm^{-2}. This graph also shows that the calculated maximum current with the traditional 33 wt % Nafion^{TM} is about 0.33 A cm^{-2} at a loading of 0.39 mg Pt cm^{-2}, in agreement with experimental results.

Other types of catalyst available (40% Pt/C and 60% Pt/C) were evaluated for optimum Nafion^{TM} content and catalyst loading; a comparison is shown in Figure 7. Maximum current increases with increasing platinum percent on carbon. However, the necessary loading to achieve those currents also increases. There is a 21% increase in the maximum current between 20% Pt/C and 60% Pt/C and a 340% increase (4.4 times increase) in the platinum loading.

Two other groups have recently performed studies on optimized electrode structures. Antolini et al. [35] developed an empirical expression that summarized their experiments to find the optimum Nafion^{TM} fraction in the active layer. They concluded from a limited number of experiments that the Nafion^{TM} to carbon weight ratio should remain constant at 0.56. They do not specify the operating conditions at which the optimization took place. The optimum Nafion^{TM} to carbon ratios in Figure 7 indicate 0.72. The higher ratio predicted here compared with Antolini might result from optimizing at a different operating potential or oxygen concentration.

Table 5. Dependence of mass transfer and kinetic parameters in cathode active layer on the Nafion^{TM} volume fraction. 20% Pt/Vulcan mixed with Nafion 1100 operating at $T = 50$ °C with air

Parameter/A cm^{-2}	Functionality based on polymer content
α_{cat}	$\frac{0.024 x_{O_2} P}{L_{cat}}(1-\varepsilon_{poly})^{1.5}$
σ_{cat}	$\frac{0.0026\,\varepsilon_{poly}}{L_{cat}}$
v for (20% Pt/C)	$1.6\times10^{-7} x_{O_2} P L_{cat} \varepsilon_{poly} \rho \exp\left[\frac{1.23-E_{cat}}{0.027}\right]$
α_{aggl}	$4.5\times10^{3} x_{O_2} P L_{cat} \varepsilon_{poly}$

$\rho = \left[\sum_i \frac{x_i^*}{\rho_i}\right]^{-1}$ where $\rho_{Pt} = 21\,000$ mg cm^{-3}, $\rho_{Nafion} = 2000$ mg cm^{-3}, and $\rho_{carbon} = 500$ mg cm^{-3}

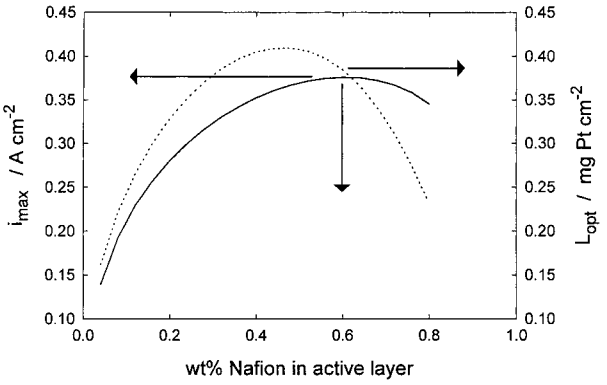

Fig. 6. Maximum current and optimum catalyst loading in the active layer as a function of the wt % Nafion^{TM} for 0.7 V, air, 20% Pt/C catalyst, $R_{mem} = 0.2\ \Omega\ cm^2$, and $\alpha_{sub} = x_{oxy}$ 12 A cm^{-2}. Key: (—) maximum current; (· · ·) optimum loading.

Marr and Li [36] performed a numerical modeling study (without any experiment) and concluded that the optimum polymer content depended on the operating current (or potential). They assumed a functionality of the transport parameters based on a void fraction in the active layer, and their results do not reflect experimental quantities found in Table 5. However, their work agrees that the optimum polymer fraction is more complex than just a ratio of the carbon to polymer weight. The optimization procedure introduced here is an improvement over both previous studies.

Equations 13 and 14 can also predict electrode performance with improved electrode materials. If the membrane resistance can be reduced to 0.05 Ω cm^2 (which is the inherent resistance of the Nafion 112 membrane), the electrode performance can be improved as shown in Figure 8. In this case, the maximum current is 0.62 A cm^{-2} at 0.7 V from a cathode containing 65 wt % Nafion^{TM} and a platinum loading of 0.20 mg Pt cm^{-2}. This type of performance has been the goal for commercialization, but has not yet been reached experimentally because of low amounts of polymer in the

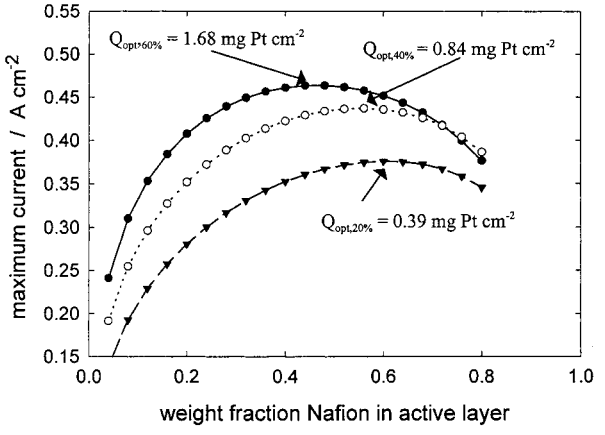

Fig. 7. Comparison of maximum currents at 0.7 V for the different platinum on carbon E-Tek catalysts and current electrode materials. Air/H_2 at atmospheric pressure and 50 °C. Key: (–●–) 60% Pt/C; (· · ○ · ·) 40% Pt/C; (–▼–) 20% Pt/C.

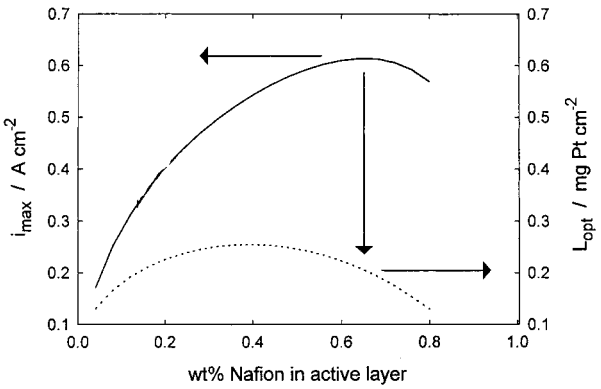

Fig. 8. Same as Figure 6 except $R_{mem} = 0.05\ \Omega\ cm^2$ which increases the maximum current and lowers the optimum loading. Key: (—) maximum current; (····) optimum loading.

active layer, problems with manufacturing, and high membrane resistance due to low water saturation.

It may be possible in the near future to obtain as high as 0.89 A cm^{-2} at 0.7 V with air at atmospheric pressure and 0.2 mg Pt cm^{-2} loading. Improvements include: the membrane resistance reduced to 0.0125 Ω cm^2 (which is the inherent resistance of the new Gore Select^{TM} 12 μm membrane [37]), the ionic conductivity of the active layer polymer improved by 50% (using a lower equivalent weight ionomer), and the substrate limiting current increased to 5 A cm^{-2} (by metal foam flow fields and the removal of the cloth/paper substrate [38]). At 0.6 V (dropping the hydrogen fuel efficiency to 48%), 1.7 A cm^{-2} could be obtained with such a cathode consisting of 63 wt % Nafion^{TM} and 0.07 mg Pt cm^{-2}. This type of performance would allow cell power densities of 3.4 kW litre^{-1} (not including cooling plates, endplates, or intercell gas distributors) with very low catalyst loading.

4. Conclusions

Based on the effectiveness factor, a method has been developed to identify the relative severity of mass transfer limitation of an existing electrode design or screen a new material for its transport feasibility. The evaluation compares inherent mass transfer coefficients and is independent of the reaction kinetics. An existing electrode design can be analysed by comparing the possible currents or effectiveness from each of the mass transfer processes to identify which processes need to be improved. New fuel cell materials can be screened before an electrode is assembled using this method by determining if the mass transfer rates are sufficient to obtain the desired operating current.

Simple expressions have been derived to calculate the maximum current and optimum thickness of the active layer with proton migration and reactant diffusion mass transfer losses. The optimum thickness represents a point that achieves close to the maximum theoretical current, at reasonable catalyst utilization. The optimum thickness and maximum current are calculated as functions of the inherent mass transfer coefficients and the intrinsic kinetic rate. An excellent correlation was obtained between these equations and experiment in spite of the simplicity of the expressions. They are accordingly much more useful for optimization than the experimental trial-and-error approach or complex numerical fits in previously published models. The use of these equations has the potential to save considerable experimental time and cost for optimizing fuel cell electrodes.

The design equations predicted performance of low catalyst loading cathodes with existing materials could be significantly improved by increasing the amount of Nafion^{TM} in the active layer from the standard 33% to about 60 wt % with the 20% Pt/C catalyst. Such an electrode operating on hydrogen and air at atmospheric pressure was shown to achieve 0.38 A cm^{-2} at 0.7 V with 0.39 mg Pt cm^{-2}. By combining recent improvements in membrane conductivity, substrate diffusivity, and active layer proton conductivity, the design equations predict that a cell should obtain 0.89 A cm^{-2} at 0.7 V with 0.2 mg Pt cm^{-2} operating on hydrogen and air at atmospheric pressure.

Acknowledgement

The authors would like to thank Dr Sergei Gamburzev for his assistance in fabricating the MEAs in this study and Mr Jeff Wallace for his assistance with testing the cells.

References

1. S. Srinivasan and R. Mosdale, *Bull. Electrochem.* **12** (1996) 170.
2. T. Ralph, G. Hards, J. Keating, S. Campbell, D. Wilkinson, M. Davis, J. St-Pierre and M. Johnson, *J. Electrochem. Soc.* **144** (1997) 3845.
3. M. Uchida, Y. Fukuoka, Y. Sugawara, N. Eda and A. Ohta, *J. Electrochem. Soc.* **143** (1996) 2245.
4. D.M. Bernardi and M.W. Verbrugge, *AIChEJ.* **37** (1991) 1151.
5. T.E. Springer, T.A. Zawodzinski and S. Gottesfeld, *J. Electrochem. Soc.* **138** (1991) 2334.
6. T.F. Fuller and J. Newman, *J. Electrochem. Soc.* **140** (1993) 1218.
7. T.V. Ngugen and R. White, *J. Electrochem. Soc.* **140** (1993) 2178.
8. J.C. Amphlett, R.M. Baumert, R.F. Mann, B.A. Peppley and P.R. Roberge, *J. Electrochem. Soc.* **142** (1995) 1.
9. D. Bevers, M. Wohr, K. Yasuda and K. Oguro, *J. Appl. Electrochem.* **27** (1997) 1254.
10. M.L. Perry, J. Newman and E.J. Cairns, *J. Electrochem. Soc.* **145** (1998) 5.
11. S. Srinivasan, H.D. Hurwitz and J.O'M. Bockris, *J. Chem. Phys.* **46** (1967) 3108.
12. J. Giner and C. Hunter, *J. Electrochem. Soc.* **116** (1969) 1124.
13. M. Viitanen and M.J. Lampinen, *J. Power Sources* **32** (1990) 207.
14. K.A. Striebel, F.R. McLarnon and E.J. Cairns, *Ind. Engr. Chem. Res.* **34** (1995) 3632.
15. S.C. Yang, M.B. Cutlip and P. Stonehart, *Electrochim. Acta* **35** (1990) 869.
16. P. DeVidts and R.E. White, *J. Electrochem. Soc.* **144** (1997) 1343.

17. T.E. Springer, M.S. Wilson and S. Gottesfeld, *J. Electrochem. Soc.* **140** (1993) 3513.
18. Y.W. Rho and S. Srinivasan, *J. Electrochem. Soc.* **141** (1994) 2089.
19. T.E. Springer, T.A. Zawodzinski, M.S. Wilson and S. Gottesfeld, *J. Electrochem. Soc.* **143** (1996) 587.
20. N. Sugumaran and A.K. Shukla, *J. Power Sources* **39** (1992) 249.
21. C. Olaman, M. Matte and C. Lum, *J. Electrochem. Soc.* **138** (1991) 2330.
22. A. Parthasarathy, B. Dave, S. Srinivasan, A.J. Appleby and C.R. Martin, *J. Electrochem. Soc.* **139** (1992) 1635.
23. C.Y. Yuh and J.R. Selman, *AIChE J.* **34** (1988) 1949.
24. T.E. Springer and I.D. Raistrick, *J. Electrochem. Soc.* **136** (1989) 1594.
25. C.C. Boyer, S. Gamburzev, O. Velev, S. Srinivasan and A.J. Appleby, *Electrochim. Acta* **43** (1998) 3703.
26. J. Muhovski, Il. Ileiv and E. Budevski, *Com. Chem.: Bulgarian Academy of Sciences* **14** (1981) 370.
27. S.K. Zecevic, J.S. Wainright, M.H. Litt, S.Lj. Gojkovic and R.F. Savinell, *J. Electrochem. Soc.* **144** (1997) 2973.
28. A. Parthasarathy, S. Srinivasan, A.J. Appleby and C.R. Martin, *J. Electrochem. Soc.* **139** (1992) 2856.
29. F.N. Buchi, A. Marek and G.G. Scherer, *J. Electrochem. Soc.* **142** (1995) 1895.
30. L. Qingfeng, X. Gang, H.A. Hjuler, R.W. Berg and N.J. Bjerrum, *J. Electrochem. Soc.* **142** (1995) 3250.
31. S.E. Lyke and S.H. Langer, *J. Electrochem. Soc.* **138** (1991) 2327.
32. F. Gloaguen and R. Durand, *J. App. Electrochem.* **27** (1997) 1029.
33. D.B. Sepa, M.V. Vojnovic and A. Damjanovic, *Electrochim. Acta* **32** (1987) 129.
34. C. Boyer, Doctoral Dissertation, Texas A&M University, College Station (1999).
35. E. Antolini, L. Giorgi, A. Pozio and E. Passalacqua, *J. Power Sources* **77** (1999) 136.
36. C. Marr and X. Li, *J. Power Sources* **77** (1999) 17.
37. O. Savadogo, *J. New Mat. Electrochem. Sys.* **1** (1998) 47.
38. S. Gamburzev, C. Boyer and A. J. Appleby, *Fuel Cells Bulletin* No. 9 (1999) 6.